PHYSICAL REVIEW B VOLUME 45, NUMBER 1 1 JANUARY 1992-I

Magnetism of Fe impurities in alkaline-earth metals and Al

Diana Guenzburger
Centro Brasileiro de Pesquisas Físicas, Conselho Nacional de Desenvolvimento Científico e Tecnológico,
Rua Dr. Xavier Sigaud, 150, 22290 Rio de Janeiro, Rio de Janeiro, Brazil

D. E. Ellis
Department of Physics and Astronomy and Materials Research Center, Northwestern University, Evanston, Illinois 60208

(Received 25 June 1991)

First-principles electronic-structure calculations were performed for embedded clusters representing an Fe impurity in the metal hosts Be, Mg, Ca, Sr, and Al. The discrete-variational method was employed in the framework of local-spin-density theory. *Be*Fe was found to be nonmagnetic, as well as *Al*Fe, this last if local relaxation is taken into account. For Fe in the other alkaline-earth metals, local magnetic moments $>2\mu_B$ were encountered. Mechanisms leading to moment stability or moment quenching are discussed. The contact hyperfine field at the Fe nucleus in *Ca*Fe was calculated, and a small positive value was found. Magnetic susceptibilities were estimated employing the virtual-bound-state model, with parameters derived from the calculations.

I. INTRODUCTION

The problem of localized magnetic moments (μ) of impurities in metallic hosts attracted great interest in the 1960s and early 1970s, being the subject of numerous experimental and theoretical efforts.[1] In spite of the considerable amount of work, the understanding of this problem is far from complete and many questions have been left unanswered.

Experiments devised to investigate the magnetism of dilute alloys include both bulk[2] (macroscopic) and local properties.[3] On the theoretical side, the "virtual-bound-state" (VBS) model of Friedel[4] and Anderson[5] provided a basis for the understanding of what conditions would lead to the existence of stable moments of transition-element impurities in *s*-*p* metals. In this model the transition impurity *d* level is broadened by interaction with the host conduction band, resulting in a resonance near the Fermi level. The existence or not of local magnetism would depend on a delicate balance between the impurity (*d*)–host (*s*-*p*) hybridization and the intraatomic correlation energy.

The VBS model provided a static picture for $T=0$; however, the discontinuity brought in by the sharp transition between magnetic and nonmagnetic regimes was sometimes found unsatisfactory. On the other hand, the theory developed by Kondo[6] and, later, Wilson[7] to explain the behavior of the resistivity of dilute alloys with temperature presented a quite different picture. According to this theory, magnetic moments, below a characteristic temperature, are screened by correlations with the conduction electrons and thus cannot manifest themselves. The Kondo theory was successful in explaining the logarithmic dependence with T of the resistivity for systems with stable magnetic moments (sometimes called "Kondo systems"). These systems have characteristic peaks in the variation with temperature of the specific heat and thermopower, and Curie-Weiss behavior of the macroscopic magnetic susceptibility.[2,8] However, at $T \rightarrow 0$ the resistivity of many alloys exhibits a T^2 dependence that cannot be accounted for by the Kondo theory.[8,9] This behavior was better explained in the context of the theory of spin fluctuations,[10] which postulates for the impurity spin a lifetime τ, which may be very short for systems with unstable moments.

The concepts of the Kondo and spin-fluctuation theories may be unified in the sense that a characteristic temperature T_K separates regions in which magnetic behavior may be detected or not. Alloys with unstable local moments are expected to have very high characteristic temperatures and thus do not display Curie-Weiss behavior of the susceptibility and other manifestations of stable moments. However, many experimental details are left unexplained and the exact microscopic description of the local moment is not given. When experiments show no sign of magnetism, one is left with the question of whether a magnetic moment is screened or very rapidly fluctuating, or whether it actually does not exist.

In recent years alternative new ways of approaching the impurity problem have become available. On the experimental side, many techniques developed for preparing alloys, such as sputtering, splat quenching, microwave sputtering, etc., have increased the number of possibilities regarding their composition and concentration. Moreover, experiments have been reported[11] in which the ion-implantation method is coupled to a precise technique probing local magnetic properties in extremely dilute limits [time-differential perturbed γ-ray angular distribution (TDPAD)]. This method has allowed the investigation of local magnetic properties of dilute impurities in hosts where alloying by more conventional methods is very difficult or not possible, mainly because of the large differences between the sizes of the impurity atom and atoms in the host crystals.

On the theoretical side, first-principles methods based on local-spin-density theory have been developed which may be used in the investigation of the electronic structure and magnetic properties of dilute impurities in metals, such as the embedded-cluster method[12–14] and the Green's-function Korringa-Kohn-Rostoker[15,16] (KKR) method. Such methods do not rely on parametrization of any kind, giving thus reliable results which may improve the microscopic understanding of the electronic nature of the impurity-host system.

We describe first-principles local-spin-density (LSD) self-consistent electronic-structure calculations for embedded clusters representing Fe impurities in the hosts Be, Mg, Ca, Sr, and Al. Magnetic properties of the Fe impurity have been investigated experimentally in all these cases by γ-ray distribution techniques following heavy-ion reactions and recoil implantation.[11] For the hosts Be and Al, the solubility of Fe on the Be- or Al-rich side of the phase diagram is very small.[17] However, very dilute solutions may also be obtained by standard alloying methods, and thus experimental results by other techniques have also been reported. For Mg, Ca, and Sr, only by ion implantation may Fe atoms be inserted in the host.[11] There is evidence that supports the hypothesis that the implanted impurities occupy substitutional sites.[18]

Among the hosts chosen for this study, Be, Mg, Ca, and Sr are alkaline-earth metals whose lattice constants cover a wide range of values and so constitute cases in which the effect of this parameter may be assessed. On the other hand, dilute alloys of Fe in the *s-p* host Al are usually considered a classical example of a system in which the spin-fluctuation temperature is very high, and so the Fe impurity behaves as nonmagnetic in all experimental circumstances.[2,8] From the TDPAD experiments, this temperature is estimated to be $> 10^4$ K.[11]

By performing self-consistent spin-polarized calculations for the impurity-host systems, the existence of a local magnetic moment was determined, as well as its magnitude when present. Results are related to the electronic properties, especially regarding the local bonding to the impurity atom. Relaxation around the impurity atom in *Al*Fe was also taken into account by performing total-energy calculations to determine the Fe nearest-neighbor equilibrium distance. Clusters of different sizes were considered in some cases to verify the convergence of the properties studied. The contact hyperfine field at the Fe nucleus was calculated for *Ca*Fe. Finally, macroscopic paramagnetic susceptibilities, defined with the aid of an extension to the Anderson model,[5] were calculated, using parameters obtained from the calculations.

In Sec. II we give some details of the theoretical method employed, in Sec. III we describe and analyze the results, and in Sec. IV we summarize our conclusions.

II. THEORETICAL METHOD

The substitutional dilute alloys were represented by clusters containing one Fe atom at the center and two or three shells of host atom neighbors. Be and Mg have hcp crystal lattices, whereas Ca, Sr, and Al have fcc structures. Hence all hosts considered have closely packed atomic arrangements.

We obtained the electronic structure of the clusters using a linear combination of atomic orbitals (LCAO) discrete-variational method (DVM),[19] within the framework of density-functional theory and the local-spin-density approximation.[20] In constructing the self-consistent potential, the charge density of several shells of atoms surrounding the cluster in the crystal is included, creating an embedding potential and thus diminishing spurious effects of simulating the solid by a cluster of atoms. The charge density of the exterior atoms is obtained by self-consistent local-density atomic calculations for approximately the configuration obtained in the cluster for the host atoms. Localization of cluster orbitals due to the Pauli exclusion principle is simulated by truncation at the core region of the potential of the exterior atoms.[21]

Self-consistent one-electron wave functions for the clusters were derived by solving iteratively the equations

$$(h_\sigma - \varepsilon_{i\sigma})\phi_{i\sigma} = (-\nabla^2/2 + V_C + V_{\mathrm{xc}}^\sigma - \varepsilon_{i\sigma})\phi_{i\sigma} = 0 \,, \tag{1}$$

where the one-electron Hamiltonian (in Hartree a.u.) includes the electron-nucleus and electron-electron Coulomb potential V_C and the spin-dependent exchange-correlation potential V_{xc}^σ derived by von Barth and Hedin.[22] This last is a function of the electron density for each spin σ, $\rho_\sigma(\mathbf{r})$, given by

$$\rho_\sigma(\mathbf{r}) = \sum_i n_{i\sigma} |\phi_{i\sigma}(\mathbf{r})|^2 \,. \tag{2}$$

In the spin-polarized calculations, ρ_σ has the freedom to be different for each spin σ. In Eq. (2), $n_{i\sigma}$ is the occupation of the cluster spin orbital $\phi_{i\sigma}$, chosen according to Fermi-Dirac statistics.

The cluster spin orbitals are expanded as a linear combination of numerical symmetrized atomic orbitals χ_j^s:

$$\phi_{i\sigma}(\mathbf{r}) = \sum_j \chi_j^s(\mathbf{r}) C_{ji}^\sigma \,, \tag{3}$$

and the variationally derived secular equations, to be solved self-consistently, are[23]

$$([H] - [E][S])[C] = 0 \,, \tag{4}$$

where $[H]$ is the energy matrix, $[S]$ the overlap matrix, and $[C]$ the matrix of the eigenvectors. All matrix elements are calculated numerically on a three-dimensional grid, which is pseudorandom in the valence region and regular polynomial in the Fe-atom core region, to assure greater precision.

In the variational expansion of the cluster spin orbitals $\phi_{i\sigma}$, all atomic orbitals are included for the Fe atom, as well as for Be. For Mg and Al only the 3*s* and 3*p* orbitals are kept in the variational basis, for Ca the 3*d*, 4*s*, and 4*p* orbitals are included, and for Sr the 4*d*, 5*s*, and 5*p*. The remaining core orbitals of the host atoms are used to build the cluster potential, but are "frozen" after the first cycle. The valence orbitals are orthogonalized with respect to the core.

The basis functions are adapted to the solid by considering the atomic configurations obtained for the clusters when generating the atomic orbitals for the LCAO expansion. To facilitate the computational procedure for building the cluster potential, the exact cluster charge density was fitted to a model variational charge density:[24]

$$\rho(\mathbf{r})\cong\rho^{M}(\mathbf{r})=\sum_{n,l,I} d_{nl}^{I}\rho_{nl}^{I}(\mathbf{r}) , \tag{5}$$

where $\rho(\mathbf{r})$ is the total electron density $\rho_{\uparrow}+\rho_{\downarrow}$; an equivalent expansion is made for the spin density $\rho_{\uparrow}-\rho_{\downarrow}$. $\rho_{nl}^{I}(\mathbf{r})$ are overlapping charge densities centered at each atom q, calculated with the radial atomic functions of the basis

$$\rho_{nl}^{I}(\mathbf{r})=\sum_{q}{}' \, |R_{nl}^{q}(r_q)|^2 Y_0^0(\hat{\mathbf{r}}_q) , \tag{6}$$

where the summation is over a previously defined set of atoms and I represents a particular set. In the present calculations, the central Fe atom forms a set by itself, and the atoms of each coordination shell of neighbor host atoms form additional sets. The coefficients d_{nl}^{I} in Eq. (5) are determined variationally in each cycle by a least-squares error-minimization procedure, with the condition that $\rho^{M}(\mathbf{r})$ integrates to the total number of electrons in the cluster. Self-consistency is achieved through convergence of these coefficients, since they ultimately determine the cluster potential.

An expansion of the charge density including higher-order multipoles is possible within the DVM method.[24] However, the present superposition of spherical charges ia adequate for close-packed metals such as those considered here. No radial truncation of the spherical charge densities is done here, in contrast to the case when adopting the "muffin-tin" approximation.

Since we are dealing with finite clusters, we obtain a discrete set of levels, which are filled with electrons according to the Aufbau principle and Fermi-Dirac statistics. A thermal "smearing" of the occupation of the levels near the Fermi energy is adopted (~0.13 eV) to assure smooth convergence. To define a partial density of states $D_{nl\sigma}^{q}(E)$ of spin σ, the levels are broadened by Lorentzians with a convenient half-width δ:

$$D_{nl\sigma}^{q}(E)=\sum_{i} P_{nl\sigma,i}^{q}\frac{\delta/\pi}{(E-\varepsilon_{i\sigma})^2+\delta^2} , \tag{7}$$

where $P_{nl\sigma,i}^{q}$ is the Mulliken population[25] of atomic orbital χ_{nl} of atom q in the cluster spin orbital $\phi_{i\sigma}$. The total density of states of spin σ is then

$$D_{\sigma}(E)=\sum_{q,n,l} D_{nl\sigma}^{q}(E) . \tag{8}$$

In one case (FeAl$_{42}$, representing *Al*Fe), total-energy calculations were performed to take into account the relaxation of the first shell of nearest neighbors (NN's) around the Fe impurity and determine the Fe-NN equilibrium distance. The total energy E_{Ω} associated with a given volume Ω with nuclei at positions $\{\mathbf{R}_{\nu}\}$ is defined as the expectation value (sum over integration mesh) of the energy density of $e(\mathbf{r},\{\mathbf{R}_{\nu}\})$ over the volume. In order to control numerical errors, the actual computation of E_{Ω} is made via point-by-point subtraction of a reference system of *noninteracting* (NI) atoms located at cluster and host (embedding) sites:[26]

$$E_{\Omega}=\langle e(\mathbf{r},\{\mathbf{R}_{\nu}\})-e^{\mathrm{NI}}(\mathbf{r},\{\mathbf{R}_{\nu}\})\rangle_{\Omega}+E_{\Omega}^{\mathrm{NI}} . \tag{9}$$

A convenient form for $e(\mathbf{r},\{\mathbf{R}_{\nu}\})$ is

$$e(\mathbf{r},\{\mathbf{R}_{\nu}\})=\sum_{\sigma}\Bigg[\rho_{\varepsilon,\sigma}(\mathbf{r})-\tfrac{1}{2}\Bigg[\rho_{\sigma}(\mathbf{r})+\sum_{\nu}{}' Z_{\nu}\delta(\mathbf{r}-\mathbf{R}_{\nu})\Bigg]V_c(\mathbf{r})+\rho_{\sigma}(\mathbf{r})[\epsilon_{\mathrm{xc}}(\mathbf{r})-\mu_{\mathrm{xc},\sigma}(\mathbf{r})]\Bigg] , \tag{10}$$

where the single-particle energy is

$$\rho_{\varepsilon,\sigma}(\mathbf{r})=\sum_{i} n_{i\sigma}\varepsilon_{i\sigma}|\psi_{i\sigma}(\mathbf{r})|^2 , \tag{11}$$

and is partitioned into atom-localized contributions in a manner similar to Eq. (5). This step introduces no errors, since the partitioning is constructed so as to leave the total (integral) single-particle energy invariant. The second term in Eq. (10) represents corrections to the Coulomb energy due to electron-electron and nuclear-nuclear repulsion; in the third term, ϵ_{xc} and μ_{xc} are the exchange-correlation energy density and chemical potential, respectively.[20] The sum and δ function in Eq. (10) restrict the nuclear contributions to sites within the integration volume. The prime in the summation leaves out self-interaction of the nuclei.

In numerical evaluation of Eq. (10), the least-squares-determined model densities are used, consistent with the self-consistent-field (SCF) procedure.

A total of ~19 500 points for the SCF procedure were found to be sufficient for the 43 atoms clusters of the fcc lattices and 9000–12 500 for the 27 atoms clusters of the hcp lattices. For the total-energy calculations of FeAl$_{42}$, 19 500 points were also found to be adequate, with a different sampling. Uncertainties in $\varepsilon_{i\sigma}$ and E_{Ω} due to numerical sampling are estimated as ~0.05 and ~0.5 eV, respectively. Since the errors remain nearly constant for small nuclear displacements, meaningful comparisons can be made for E_{Ω} vs $\{\mathbf{R}_{\nu}\}$.

III. RESULTS AND DISCUSSION

A. Charge transfer and magnetic moments

In Table I we give some general information on the systems investigated, such as crystal structures, lattice parameters, Pauling electronegativities, and atomic radii of the hosts. The same is given for bcc Fe for comparison. We also list the clusters considered to represent each dilute alloy, indicating the number of host atoms in the first-neighbor shell of the Fe atom (NN), second, and, in some cases, third shell. The 19-atom cluster for fcc

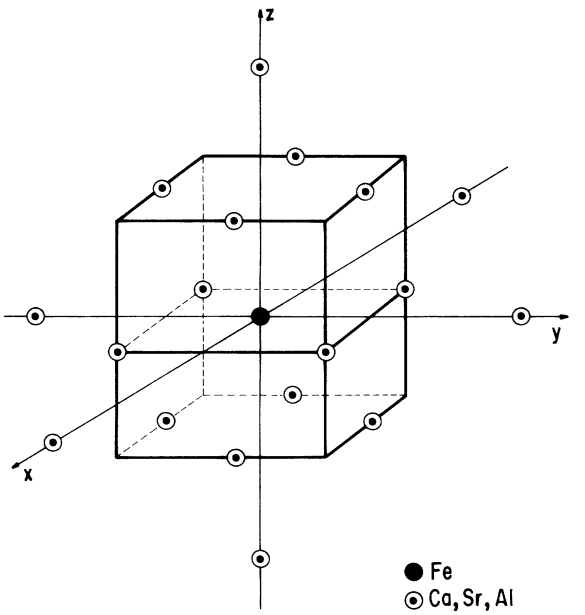

FIG. 1. Representation of the 19-atom cluster for the fcc lattice.

hosts ($FeM_{12}M_6$) is depicted in Fig. 1 and the 27-atom cluster representing the hcp alloys ($FeM_{12}M_{14}$) is represented in Figs. 2(a) and 2(b). Larger clusters ($FeM_{12}M_6M_{24}$) were also considered for Fe in the fcc hosts Al and Ca.

In Table I are also given the charges on the Fe impurity atom; these were obtained by a Mulliken population[25] analysis of the LCAO wave functions of the clusters. A definition of "charge" or "moment" of an atom in a solid is necessarily arbitrary, since the atom's properties obviously cannot be isolated from those of the host. For this reason one should focus preferably on trends rather than absolute numbers. Here we have chosen to use the Mulliken population definition, according to which atomic orbital populations are roughly proportional to the

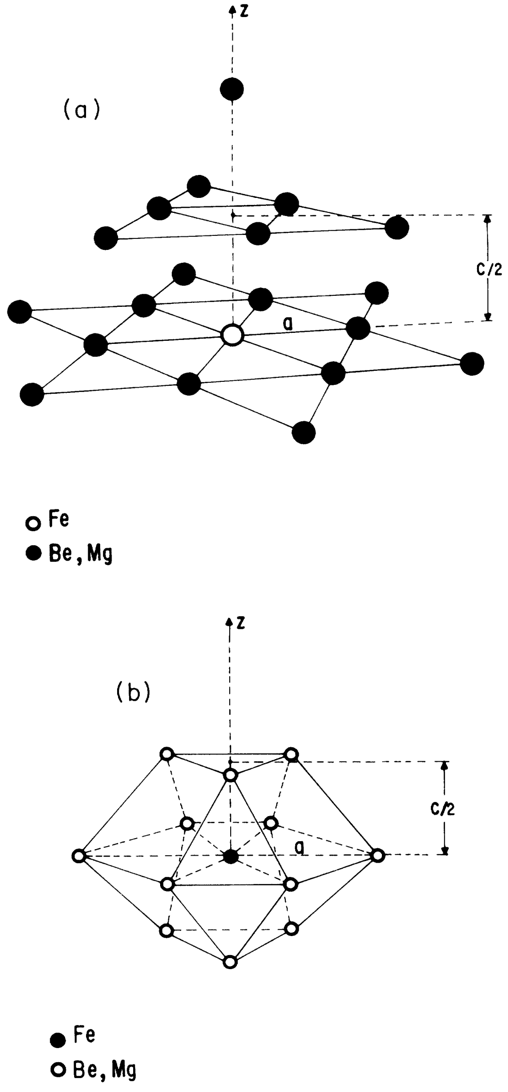

FIG. 2. (a) Upper portion of the 27-atom cluster representing the hcp alloys. (b) Impurity and NN shell of host atoms of the hcp alloys.

TABLE I. Crystal structure, lattice parameters, atomic radii, and Pauling electronegativities of hosts, clusters considered, Mulliken and volume charges of Fe, magnetic moments on Fe, and total cluster magnetic moments. (a) For the Al lattice interatomic distances. (b) Equilibrium Fe-NN interatomic distance.

Host metal	Crystal structure	Lattice parameters (Å)	Host atomic radius (Å)	Pauling electronegativity of host	Clusters	Mulliken charge on Fe	Volume charge on Fe	Magnetic moment on Fe(μ_B)	Cluster magnetic moment (μ_B)
Be	hcp	$a=2.29$ $c=3.58$	1.11	1.5	$FeBe_{12}Be_{14}$	1.64−	0.62+	0	0
Mg	hcp	$a=3.21$ $c=5.21$	1.60	1.2	$FeMg_{12}Mg_{14}$	0.64−	0.44−	2.23	1.69
Ca	fcc	$a=5.58$	1.97	1.0	$FeCa_{12}Ca_6$	0.73−	0.73−	2.78	2.18
					$FeCa_{12}Ca_6Ca_{24}$	0.54−	0.48−	2.93	2.67
Sr	fcc	$a=6.08$	2.15	1.0	$FeSr_{12}Sr_6$	0.78−	0.79−	3.01	2.60
Al	fcc	$a=4.05$	1.43	1.5	(a) $FeAl_{12}Al_6$	0.98−	0.51−	0.44	0.09
					(a) $FeAl_{12}Al_6Al_{24}$	0.84−	0.49−	0.96	0.55
					(b) $FeAl_{12}Al_6Al_{24}$	0.98−	0.58−	~0	~0
Fe	bcc	$a=2.87$	1.25	1.8					

squares of the coefficients in the LCAO expansion. Magnetic moments are thus defined as the difference between spin-up and -down orbital or total populations. Along with the Mulliken charges of Fe in Table I, we also list the volume charges for comparison. These are obtained by integrating the charge density around Fe inside the Wigner-Seitz nearest volume of the host. Volume charges are also arbitrarily defined, since one cannot unambiguously determine which volume the electrons of the impurity atom are actually filling. In Table I it may be seen that for the cases in which the atomic radius of the host atoms is smaller or comparable to that of Fe, there is a considerable difference between Mulliken and volume charges. This is particularly striking in the case of *Be*Fe, where the Wigner-Seitz volume of Be is obviously too small to accommodate the Fe electrons. For the hosts with large lattice constants (the alkaline-earth metals), the two charge definitions give very similar values, especially for Ca and Sr, which have the largest atomic radii.

For the $FeAl_{42}$ cluster representing Fe in Al, a detailed study of the influence of the relaxation of the NN atoms around Fe has been performed[27] by determining the Fe-NN distance for which the total energy of the cluster has the minimum value. This investigation was motivated by the fact that recent first-principles calculations for *Al*Fe at the Al lattice distances obtained large magnetic moments on Fe [$1.78\mu_B$ (Ref. 15) and $1.73\mu_B$ (Ref. 28)], although experimental evidence, such as behavior of magnetization with temperature,[29] seems to point to a nonmagnetic system.[2,8,9] The results of our calculations, the details of which will be published elsewhere,[27] give for Fe a moment $\mu \sim 1\mu_B$ for calculations at the Al equilibrium lattice distance (Fe-NN distance$=$2.86 Å). This moment, however, collapses to zero at the equilibrium Fe-NN distance $d \cong 2.7$ Å. In Table I we give Fe charges for the $FeAl_{42}$ cluster for calculations at both the Al lattice and equilibrium Fe-NN distances.

It may be seen that all the Mulliken charges on Fe are negative. This is consistent with the fact that the electronegativity of Fe is higher than that of the host atoms in all cases, resulting in a $M \rightarrow$Fe charge transfer. However, the charge transfer is more pronounced for the cases in which the Fe-*M* distance is smaller (Be and Al), since a shorter distance favors the impurity-host interaction. For $FeAl_{42}$, calculation (b) of Table I for the shorter Fe-NN equilibrium distance gives a larger negative charge on Fe than calculation (a) of Table I for the unrelaxed Al lattice distance.

In the next to last column of Table I are listed the magnetic moments on the Fe impurity defined, as described earlier, as the difference in the spin-up and -down Mulliken populations of Fe. In the last column are given the total cluster magnetic moments. It may be seen that these last are systematically smaller than μ of the Fe atom; this is due to the antiferromagnetic alignment of the moments of the host atoms with respect to the Fe μ.

From these calculations it is seen that Fe in Be is nonmagnetic. This is in accord with Mössbauer experiments in the presence of an external magnetic field,[30] which give for μ(Fe) an upper bound of $0.01\mu_B$. Furthermore, TDPAD experiments for Fe implanted in Be show nonmagnetic characteristics, which were interpreted as deriving from a very high spin-fluctuation instability ($T_K > 10^4$ K).[11]

For all other hosts and calculations performed at the host lattice distances, a magnetic moment is found on the Fe impurity. This moment is larger than $2\mu_B$ for the alkaline-earth metal hosts and is about $1\mu_B$ for the $FeAl_{42}$ cluster representing *Al*Fe. For the only case in which the effect of the local lattice relaxation on μ was investigated in detail, which is the $FeAl_{42}$ cluster, it was found that at the Fe-NN equilibrium distance the moment has collapsed to zero[27] [case (b) in Table I].

TDPAD experiments performed for Fe implanted in Mg, Ca, and Sr showed evidence of more stable local moments than in *Be*Fe; results were scaled to lower T_K values ($\sim 10^3$ K).[11] For Fe in Al, the same experiments were interpreted assuming $T_K > 10^4$ K. A large positive magnetic hyperfine field was found[31] for dilute Fe in Ca with the perturbed angular distribution technique.

The effect of cluster size was investigated for *Ca*Fe and

TABLE II. Mulliken populations and charges. Fe (3*s*) and (3*p*) populations, not included in table, show small deviations from the free-atom values. (a) For the Al lattice interatomic distances. (b) Equilibrium Fe-NN interatomic distance.

Host		Be	Mg	Ca	Sr	(a) Al	(b) Al
Cluster		$FeBe_{26}$	$FeMg_{26}$	$FeCa_{42}$	$FeSr_{18}$	$FeAl_{42}$	$FeAl_{42}$
Orbital populations on Fe	3*d*	7.95	7.58	7.13	6.99	8.03	8.14
	4*s*	0.88	0.84	1.16	1.40	0.59	0.57
	4*p*	0.86	0.23	0.26	0.39	0.24	0.32
Orbital populations on NN atom		2*s* 0.83	3*s* 1.35	3*d* 0.47	4*d* 0.55	3*s* 1.45	3*s* 1.42
		2*p* 1.04	3*p* 0.61	4*s* 0.85	5*s* 1.09	3*p* 1.49	3*p* 1.50
				4*p* 0.67	5*p* 0.32		
Charge on NN atom		0.130+	0.036+	0.007+	0.034+	0.057+	0.081+
Charge on second-shell atom		0.005+	0.015+	0.168−	0.063+	0.001+	0.004+
Charge on third-shell atom				0.061+		0.006+	0.001−

TABLE III. Orbital and total magnetic moments (in μ_B). (a) For the Al lattice interatomic distances.

Host		Mg	Ca	Sr	(a) Al
Cluster		$FeMg_{26}$	$FeCa_{42}$	$FeSr_{18}$	$FeAl_{42}$
Orbital moments on Fe	3*d*	2.10	2.74	2.85	0.92
	4*s*	0.09	0.14	0.10	0.03
	4*p*	0.03	0.06	0.07	0.02
Orbital moments on NN atom		3*s* 0.001	3*d* −0.007	4*d* −0.022	3*s* −0.001
		3*p* −0.031	4*s* −0.003	5*s* −0.001	3*p* −0.010
			4*p* −0.007	5*p* −0.004	
Total moment on NN atom		−0.030	−0.017	−0.027	−0.011
Moment on second-shell atom		−0.012	−0.003	−0.017	+0.002
Moment on third-shell atom			−0.002		−0.012

*Al*Fe, this last at the unrelaxed Al lattice distances. In both cases it is seen that increasing the cluster from 19 to 43 atoms produces an increase in μ(Fe) and μ(cluster). This effect is more pronounced for *Al*Fe.

In Table II are listed the Fe 3*d*, 4*s*, and 4*p* orbital populations, as well as orbital populations of the NN atoms and atomic charges of each host atom in the NN, second, and third shells. There is considerable Fe(4*s*,4*p*) hybridization in all cases, and the 3*d* population is considerably higher than that of the free atom ($3d^6 4s^2$). For the hosts Ca and Sr, for which the lattice constants are very large and, consequently, the impurity atom is considerably isolated, the 3*d* population tends to be smaller, as the (4*s*,4*p*) hybridization, and the Fe configuration resembles more that of the free atom. The self-consistently obtained Fe 3*d* populations may be somewhat artificially augmented because of the fact that the local-density approximation tends to favor *d* occupancy relative to *s*, in first-row transition elements.[32] On the other hand, $s \rightarrow d$ promotion is consistently found in band-structure calculations which reproduce well bulk properties.

For Fe in Ca, the charge on the host atoms has a pronounced oscillatory behavior, being positive in the NN shell, negative in the second, and positive again in the third shell of neighbors. One may also note that the *d* populations on Ca and Sr are far from negligible, indicating that these orbitals must be taken into account to describe properly the electronic structure of these metals, at least in the presence of the Fe impurity. The contraction of the NN shell in $FeAl_{42}$ [calculation (b) in Table II] produces a small ($\sim$0.1) increase in the population of the 3*d* orbital of Fe.

In Table III are displayed the individual orbital magnetic moments of Fe and the NN host atoms. Also listed are the total μ on each of the NN, second-shell, and third-shell host atoms. From this table it is seen that the 4*s* and 4*p* electrons of Fe align ferromagnetically with the 3*d* moment, contrary to what happens in Fe metal.[12,13] μ of all shells of host neighbors align antiferromagnetically with the Fe moment for *Mg*Fe, *Ca*Fe, and *Sr*Fe. The antiferromagnetic response decreases with the distance of the atom from Fe. In the calculation for $FeAl_{42}$, performed at the unrelaxed Al lattice distances, an oscillatory behavior is observed in the magnetic moments of the host atoms. In all cases the antiferromagnetism of the host atoms comes predominantly from the *p* and *d* electrons, the magnetic polarization of the *s* electrons being very small.

In Figs. 3–8 are drawn the difference in spin-up and -down total cluster and Fe densities of states (spin DOS) for the clusters representing *Mg*Fe, *Ca*Fe, *Sr*Fe, and *Al*Fe, this last at the unrelaxed Al lattice Fe-NN distance. This manner of presentation highlights the magnetic aspect of the energy-level distributions. It may be seen in the figures that the Fe spin-up energy levels are predominant at energies just below the Fermi level; ε_F is positioned among the spin-down set of levels. The most striking aspect of these diagrams is the distinction between *Al*Fe and the other systems. In fact, for the clusters representing *Mg*Fe, *Ca*Fe, and *Sr*Fe, the difference between the total cluster and Fe DOS diagrams is very small for occupied states. In contrast, the DOS diagrams of both $FeAl_{18}$ and $FeAl_{42}$ show a noticeable difference between the cluster and Fe spin DOS. In fact, in the diagram for the cluster spin DOS are seen oscillations at lower energies, as a result of predominance at certain en-

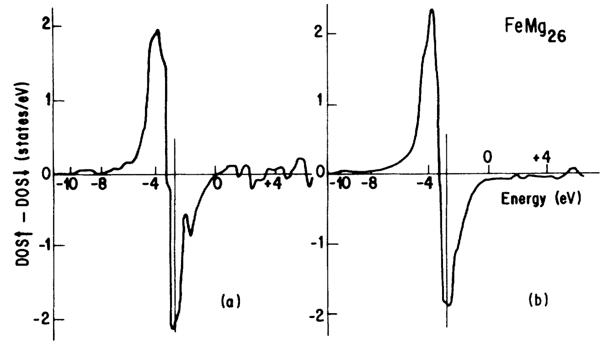

FIG. 3. Spin-up minus spin-down density of states of $FeMg_{26}$. (a) Total cluster. (b) Fe atom ($3d + 4s + 4p$).

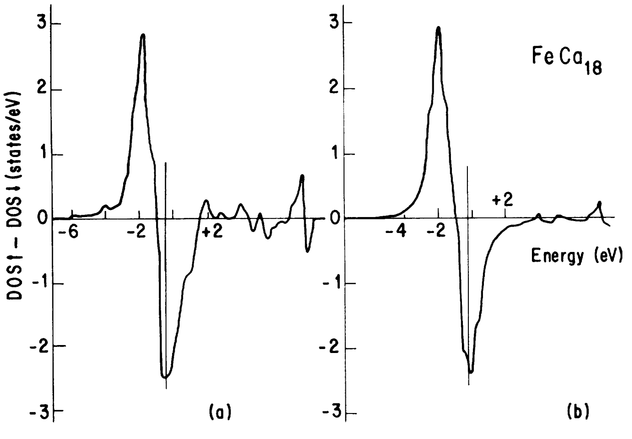

FIG. 4. Spin-up minus spin-down density of states of FeCa$_{18}$. (a) Total cluster. (b) Fe atom ($3d + 4s + 4p$).

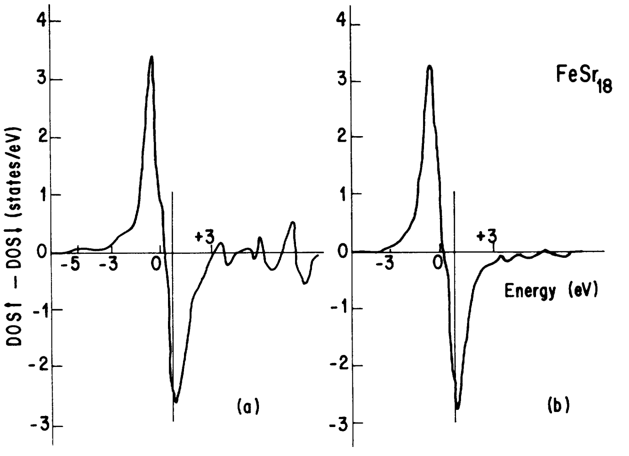

FIG. 6. Spin-up minus spin-down density of states of FeSr$_{18}$. (a) Total cluster. (b) Fe atom ($3d + 4s + 4p$).

ergy intervals of the spin-down levels of the Al host. This feature is important in explaining the relative moment stability of these systems, as will be discussed in the next section.

B. Mechanisms of moment stability

The results described so far offer the possibility of analyzing mechanisms leading to the stabilization or quenching of the magnetic moment on Fe.

First, we note in Table I that for calculations at the host lattice distances, there is an obvious correlation between impurity moment and interatomic distances. In fact, for the Be host the interatomic distances are the shortest, and the calculation gives zero moment. For *Al*Fe the situation is intermediate, and for the alkaline-earth metals the Fe moments are large and increase with increasing interatomic distances in the sequence Mg→Ca→Sr. Short Fe-NN distances allow a greater impurity-host interaction. In addition, since the electronegativity of Fe is higher than that of any of the hosts, the greater interaction allows more charge transfer into the spin-down levels of the impurity, contributing to quench the moment.

For *Al*Fe, DOS diagrams of both clusters FeAl$_{18}$ and FeAl$_{42}$ show the existence of occupied spin-down Al levels at low energies (below the Fe resonance), a feature not present in the alkaline-earth metal hosts. This must be due to the existence of the more stable atomic valence $3p$ level of Al, as compared to atomic valence p levels of the alkaline-earth atoms. As seen in Table III, p levels of the hosts are always antiferromagnetic; however, in *Al*Fe the Al $3p$ band lies lower, strongly overlapping with the Fe $3d$ states. This leads to bonding structure extending well below the simple d-band "doublet" seen for the alkaline-earth hosts: compare Figs. 3–6 with Fig. 8. The larger number of occupied host p states coupled antiferromagnetically to the Fe d moment and the larger overlap and resulting hybridization with Fe d states both act self-consistently to reduce the net moment. The relatively stronger antiferromagnetic response of the host in *Al*Fe may be verified by examining the ratio $\mu(\text{cluster})/\mu(\text{Fe})$.

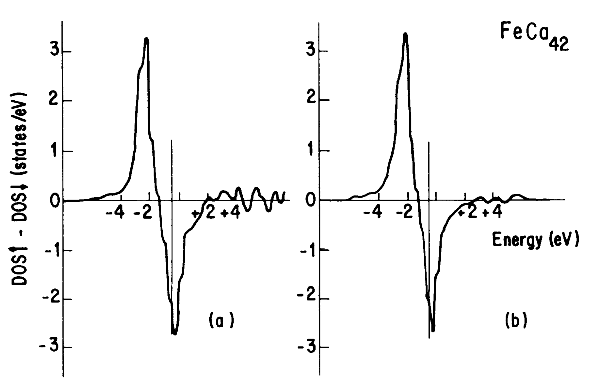

FIG. 5. Spin-up minus spin-down density of states of FeCa$_{42}$. (a) Total cluster. (b) Fe atom ($3d + 4s + 4p$).

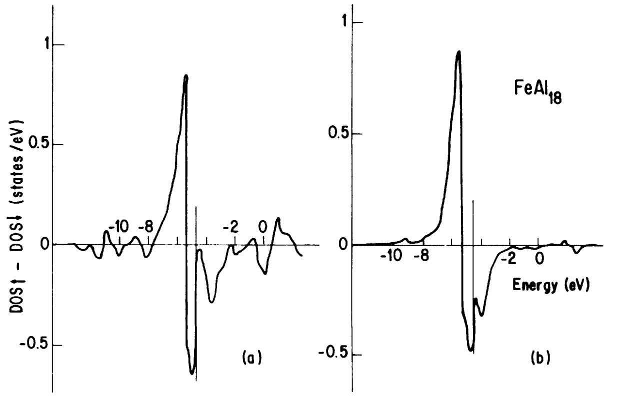

FIG. 7. Spin-up minus spin-down density of states of FeAl$_{18}$, for the Al lattice interatomic distances. (a) Total cluster. (b) Fe atom ($3d + 4s + 4p$).

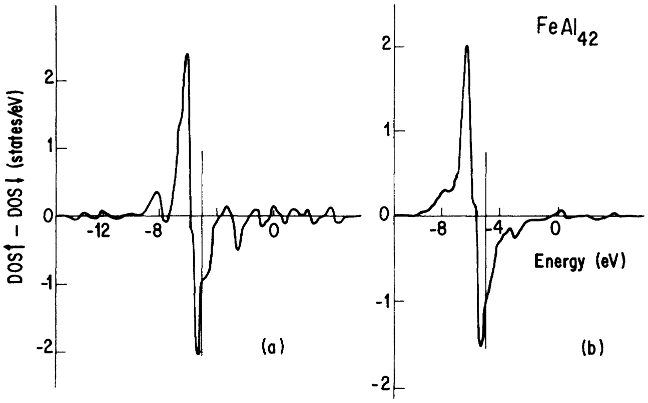

FIG. 8. Spin-up minus spin-down density of states of $FeAl_{42}$, for the Al lattice interatomic distances. (a) Total cluster. (b) Fe atom ($3d+4s+4p$).

In fact, this ratio is only 0.57 for the unrelaxed cluster $FeAl_{42}$, as compared to 0.91 for $FeCa_{42}$, 0.76 for $FeMg_{26}$, and 0.86 for $FeSr_{18}$.

As mentioned earlier, the determination of the equilibrium Fe-NN distance (2.7 Å) in $FeAl_{42}$ by total-energy calculations indicate that it is shorter than the Al lattice NN distance (2.86 Å).[27] At the distance of the minimum energy, the system is nonmagnetic. This shows the importance of relaxation for localized magnetic moments, especially in cases such as *Al*Fe that have signs of magnetic instability even at the host lattice distances, as discussed in the preceding paragraph. Previous first-principles calculations for *Al*Fe (Refs. 15 and 28) did not take local relaxation into account. In principle, the same detailed investigation of the influence of local interatomic distances should be carried out in all cases; this, however, is beyond the scope of this work. We did, however, perform a SCF calculation for $FeMg_{26}$ for a shorter Fe-NN distance, namely, ~2.9 Å (10% contraction), and saw no sign of total collapse of μ on Fe, although μ decreases: we obtained $\mu(\mathrm{Fe})\cong 1.8\mu_B$. The distance chosen (2.9 Å) corresponds approximately to the sum of the atomic radii of Fe and Mg, which, in a simple intuitive model, would be the Fe-Mg interatomic distance in the alloy. For *Al*Fe the interatomic distance at equilibrium, obtained after extensive total-energy calculations, is found to be very nearly the sum of the atomic radii of Fe and Al;[27] as mentioned previously, for this distance $\mu=0$.

C. Hyperfine field of dilute Fe in Ca

Experiments were reported for isolated Fe impurities in Ca with the perturbed angular distributions technique,[31] in which measurements of the magnetic hyperfine field H_F as a function of temperature were performed and a large positive value was encountered. In order to extract a value for the hyperfine field from experiment, it is necessary to assume values for the effective electronic spin J' and effective moment μ'. Using plausible values $J'=2$ and $\mu'\cong 2\mu_B$, one obtains $H_F\cong+150$ kOe. This was interpreted as indication of the presence of a large unquenched orbital moment. Calculations of orbital hyperfine fields are beyond the scope of this work. Instead, we were interested in verifying the contribution of the direct [or contact (Fermi)] hyperfine field to the total field measured. The contact hyperfine field H_c is defined as

$$H_c=\frac{8\pi}{3}g\mu_B\frac{1}{2}[\rho_\uparrow(0)-\rho_\downarrow(0)]\ , \tag{12}$$

where the term in brackets is the electronic spin density at the Fe nucleus, with ρ_σ given by Eq. (2).

In our calculations $\Delta\rho(0)$ of the conduction electrons was obtained directly from the $FeCa_{42}$ cluster calculation. The core contributions were obtained from atomic LSD calculations for the same configuration that Fe has in the cluster and the same exchange-correlation potential (von Barth–Hedin). This expedient is necessary since, although no Fe orbitals are frozen in the cluster calculation, the LCAO basis is not flexible enough in the core region to represent the spin-density oscillations adequately.

In Table IV are shown the results for H_c. It is seen that a delicate balance between positive and negative terms results in a small positive total H_c at the Fe nucleus. The positive H_c is consistent with the ferromagnetic alignment of the Fe($4s$) moment with respect to $3d$ (see Table III), which results in an excess majority spin $4s$ electrons at the Fe nucleus. This is in marked contrast to the case of Fe (bcc) metal, for which similar calculations[12,13] give a negative value (−53 kOe) for the contribution of the conduction electrons, mainly because of the antiferromagnetic alignment of the Fe($4s$)electrons relative to $3d$. This negative conduction-electron contribution, added to the negative core value, results in a large negative H_c for Fe metal.

The large positive conduction-electron contribution to H_c in *Ca*Fe is also consistent with the isolation of the Fe atom in the Ca lattice (with large lattice constants) and consequent large $4s$ population (see Table II), tending to the free-atom value. In fact, the contact hyperfine field of the $4s$ electrons of the free Fe atom (configuration $3d^64s^2$) was calculated to be positive.[33] The polarization caused by the $3d$ electrons tends to attract the external $4s$ majority-spin electrons toward the inner region of the atom. This results in a positive $4s$ contact field, even for an equal number of spin-up and -down electrons.

Although we find a positive value for H_c, it is too small as compared to the total positive field measured. The remaining effect may then be the (positive) orbital hyperfine field, resulting from unquenched orbital momentum.[31] In this case it will be necessary to invoke a

TABLE IV. Contributions to the contact hyperfine field at the Fe nucleus in $FeCa_{42}$ representing *Ca*Fe (in kOe).

$1s$	−17.20	Total core:	−276.47
$2s$	−508.05		
$3s$	+248.78		
	Conduction electrons		+278.93
	Total		+2.5

TABLE V. Virtual-bound-state parameters and Fe magnetic susceptibilities. Energies in eV. n_σ is the population of orbital $3d_\sigma$ of Fe. $(\varepsilon_\sigma - \varepsilon_F)$ is the position of the maximum of the DOS peak of spin σ relative to the Fermi energy. (a) For the calculation at the equilibrium Fe-NN distance. (b) From Ref. 35 at 1090 °C. (c) From Ref. 35, extrapolating to 30 °C, using the temperature dependence of *Al* Mn.

Host	Be	Mg	Ca	Sr	(a) Al
Cluster	$FeBe_{26}$	$FeMg_{26}$	$FeCa_{42}$	$FeSr_{18}$	$FeAl_{42}$
$n_\uparrow$	3.98	4.84	4.93	4.92	4.07
$n_\downarrow$	3.98	2.74	2.20	2.07	4.07
$\varepsilon_\uparrow - \varepsilon_F$	−1.91	−1.50	−1.97	−1.80	−0.85
$\varepsilon_\downarrow - \varepsilon_F$	−1.91	−0.057	+0.059	+0.105	−0.85
$\Delta_\uparrow$	1.43	0.151	0.087	0.090	0.562
$\Delta_\downarrow$	1.43	0.375	0.304	0.379	0.562
Δ (average)	1.43	0.263	0.195	0.234	0.562
$U/5$	~0.7 (estimated)	0.685	0.741	0.614	~0.7 (estimated)
χ (calculated) (10^{-6} emu/mol)	~40	252	279	218	140
χ (experimental) (10^{-6} emu/mol)					(b) 375 (c) ~230

noncubic local symmetry, which is perhaps an indication of a slight displacement of Fe from the ideal substitutional site. One should also keep in mind that the small net value resulting from the sum of positive and negative contributions makes the total balance obtained from calculations of H_c rather sensitive to the theoretical method employed.[33]

D. Macroscopic magnetic susceptibilities

In Table V are given some parameters derived from the calculations and which are useful for application of the virtual-bound-state model. It is seen in the table that the $n_\uparrow$ values [spin-up Fe(3*d*) populations] are very near the maximum value (5) for the alkaline-earth hosts Mg, Ca, and Sr.

The energy of the maximum spin-up DOS relative to the Fermi energy $(\varepsilon_\uparrow - \varepsilon_F)$ is similar in all cases except *Al*Fe. The spin-down maximum $\varepsilon_\downarrow$ is very near the Fermi level for Fe in Mg, Ca, and Sr.

An x-ray photoemission spectroscopy (XPS) investigation of *Al*Fe has been reported.[34] The experimental value found for $|\varepsilon_\sigma - \varepsilon_F|$ is in very good agreement with our calculated value (0.9 eV, as compared to calculated 0.85 eV). The half-width of the VBS resonance level (Δ) obtained from the XPS spectrum is somewhat wider than our value (0.75 eV, as compared to calculated 0.56 eV).

We have calculated half-widths from the relation[5] (where n_σ is the population of the $3d_\sigma$ orbital of Fe)

$$\Delta_\sigma = \tan(\pi n_\sigma / 5)(\varepsilon_\sigma - \varepsilon_F) , \tag{13}$$

and the effective correlation integral $U/5$ (for each $3d_{\uparrow(\downarrow)}$ level) from

$$U/5 = \frac{\varepsilon_\uparrow - \varepsilon_\downarrow}{n_\downarrow - n_\uparrow} . \tag{14}$$

The magnetic susceptibility χ has been derived to be[5]

$$\chi = \frac{10\mu_B^2}{\Delta\pi / [\sin^2(n/5)\pi] - U} . \tag{15}$$

We have derived, in a completely analogous manner, an expression for χ for the spin-polarized case, when $n_\uparrow \neq n_\downarrow$:

$$\chi = 5\mu_B^2 \frac{\sin^2[(n_\uparrow/5)\pi] + \sin^2[(n_\downarrow/5)\pi] + (2U/\Delta\pi)\{\sin^2[(n_\uparrow/5)\pi]\sin^2[(n_\downarrow/5)\pi]\}}{\Delta\pi - (U^2/\Delta\pi)\{\sin^2[(n_\uparrow/5)\pi]\sin^2[(n_\downarrow/5)\pi]\}} , \tag{16}$$

where Δ is the average of $\Delta_\uparrow$ and $\Delta_\downarrow$. This expression reduces to Eq. (15) when $n_\uparrow = n_\downarrow = n$.

In Table V are given the values calculated for $\Delta_\uparrow$, $\Delta_\downarrow$, $U/5$, and χ, obtained by fitting the VBS parameters to the LSD energy spectrum. For the nonmagnetic case (*Be*Fe and *Al*Fe), Eq. (15) was employed, and for the magnetic cases we used Eq. (16). It is seen that $\Delta_\uparrow$ is always considerably narrower than $\Delta_\downarrow$ in the magnetic cases. This is consistent with the much wider energy extension of the spin-down levels (see Figs. 3–8), representing the greater interaction of the more extended spin-down orbitals of Fe with the host. Calculated values of U do not differ much from each other and fall in a reasonable range.

Calculated values of χ are larger for Fe in Mg, Ca, and Sr metals (magnetic systems), very small for *Be*Fe, and intermediate for *Al*Fe. Only for this last case has an experimental value been reported,[35] and this was obtained in the liquid state (1090 °C).

The calculated values for χ reported here should be viewed only regarding trends and orders of magnitude.

The approximation of a Lorentzian shape for the Fe(3*d*) spin-up and -down peaks inherent to the VBS model is very far from being accurate, as seen in Figs. 3–8. Furthermore, values of $\Delta_\downarrow$ are only crude estimates for *Mg*Fe, *Ca*Fe, and *Sr*Fe because of the use of Eq. (13) in the cases in which $\varepsilon_\downarrow$ is very near ε_F. It is possible to extend the VBS model using multiple Lorentzian lines; however, in our opinion this will add little to our understanding.

IV. SUMMARY OF CONCLUSIONS

We have performed local-spin-density calculations with the discrete-variational method for embedded clusters representing a dilute Fe impurity in the metals Be, Mg, Ca, Sr, and Al. The results obtained provide considerable insight into the mechanisms related to the existence and stability of local magnetic moments in these alloys. *Be*Fe is seen to be nonmagnetic, in accord with reported Mössbauer spectroscopy measurements. Fe in Mg, Ca, and Sr has a stable local magnetic moment. The same is true for *Al*Fe for calculations at the Al unrelaxed lattice interatomic distances; if relaxation of the NN Al atoms is taken into account, the moment collapses. Host lattice constants, antiferromagnetism of host atoms, and charge transfer are seen to relate to the existence and magnitude of the moments.

The contact hyperfine field of Fe in Ca was calculated and seen to be small and positive because of a large (positive) contribution from the Fe(4*s*) conduction electrons, which outweighs the core negative contribution. While of the correct sign to explain the highly unusual experimental situation, it is likely that other effects such as unquenched orbital magnetism connected to a lattice distortion need to be invoked to explain the experimental results. However, we note that since $H_c \gtrsim 0$, the required orbital contribution is ~ 150 kOe and not the very large values 600–700 kOe previously suggested.[31]

The virtual-bound-state model was used to estimate values for the magnetic susceptibilities. These results provide predicted trends for a comparison with future experiments and improved theories.

ACKNOWLEDGMENTS

D. E. Ellis acknowledges support from the National Science Foundation Grant No. DMR 8821571 through the Northwestern University Materials Research Center. Calculations were performed at the Cray YMP of the Pittsburgh Supercomputing center with support of NSF.

---

[1] See, for example, *Proprietés electroniques des métaux et alliages*, edited by C. Janot, M. Gerl, J. Grilhé, and J. Caisso (Masson, Paris, 1973); D. K. Wohlleben and B. R. Coles, in *Magnetism*, edited by G. T. Rado and H. Suhl (Academic, New York, 1973), Vol. V.

[2] C. Rizzuto, Rep. Prog. Phys. **37**, 147 (1974).

[3] A. Narath, in *Magnetism* (Ref. 1), Vol. V.

[4] J. Friedel, Can. J. Phys. **34**, 1190 (1956).

[5] P. W. Anderson, Phys. Rev. **124**, 41 (1961).

[6] J. Kondo, in *Solid State Physics*, edited by F. Seitz, D. Turnbull, and H. Ehrenreich (Academic, New York, 1969), Vol. 23.

[7] K. G. Wilson, Rev. Mod. Phys. **47**, 773 (1975).

[8] G. Grüner, Adv. Phys. **23**, 941 (1974).

[9] K. H. Fisher, in *Kondo and Spin-Fluctuation Systems*, edited by K. H. Hellwege, Landolt-Börnstein (Springer-Verlag, Berlin, 1982), Vol. 15, group III.

[10] A. D. Caplin and C. Rizzuto, Phys. Rev. Lett. **21**, 746 (1968); N. Rivier and J. Zitkova, Adv. Phys. **20**, 143 (1971).

[11] D. Riegel, L. Büermann, K. D. Gross, M. Luszik-Bhadra, and S. N. Mishra, Phys. Rev. Lett. **61**, 2129 (1988); **62**, 316 (1989).

[12] D. Guenzburger and D. E. Ellis, Phys. Rev. B **31**, 93 (1985).

[13] D. Guenzburger and D. E. Ellis, J. Magn. Magn. Mater. **59**, 139 (1986).

[14] B. Delley, D. E. Ellis, and A. J. Freeman, J. Magn. Magn. Mater. **30**, 71 (1982).

[15] J. Deutz, P. H. Dederichs, and R. Zeller, J. Phys. F **11**, 1787 (1981).

[16] P. J. Braspenning, R. Zeller, A. Lodder, and P. H. Dederichs, Phys. Rev. B **29**, 703 (1984).

[17] M. Hansen, *Constitution of Binary Alloys* (McGraw-Hill, New York, 1958).

[18] D. Riegel, H. J. Barth, M. Luszik-Bhadra, and G. Netz, in *Valence Instabilities*, edited by P. Wachter and H. Boppart (North-Holland, Amsterdam, 1982).

[19] D. E. Ellis and G. S. Painter, Phys. Rev. B **2**, 2887 (1970).

[20] For a review, see J. Callaway and N. H. March, in *Solid State Physics*, edited by H. Ehrenreich and D. Turnbull (Academic, New York, 1984), Vol. 38.

[21] D. E. Ellis, G. A. Benesch, and E. Byrom, Phys. Rev. B **16**, 3308 (1977).

[22] U. von Barth and L. Hedin, J. Phys. C **5**, 1629 (1972).

[23] A. Rosén, D. E. Ellis, H. Adachi, and F. W. Averill, J. Chem. Phys. **85**, 3629 (1976).

[24] B. Delley and D. E. Ellis, J. Chem. Phys. **76**, 1949 (1982).

[25] R. S. Mulliken, J. Chem. Phys. **46**, 497 (1949).

[26] P. K. Khowash and D. E. Ellis, Phys. Rev. B **39**, 1908 (1989); B. Delley, D. E. Ellis, A. J. Freeman, E. J. Baerends, and D. Post, *ibid.* **27**, 2132 (1983).

[27] D. Guenzburger and D. E. Ellis (unpublished).

[28] O. Eriksson and A. Svane, J. Phys. Condens. Matter **1**, 1589 (1989).

[29] L. Moberly, T. Steelhammer, O. G. Symko, and W. Weyhmann, J. Low Temp. Phys. **33**, 21 (1978).

[30] I. Campbell, B. Ferry, P. Imbert, and F. Varret, C. R. Acad. Sci. Paris B **271**, 749 (1970).

[31] M. H. Rafailovich, E. Dafni, H. E. Mahnke, and G. D. Sprouse, Phys. Rev. Lett. **50**, 1001 (1983).

[32] J. Harris and R. O. Jones, J. Chem. Phys. **70**, 830 (1979).

[33] D. Guenzburger, D. M. S. Esquivel, and J. Danon, Phys. Rev. B **18**, 4561 (1978).

[34] P. Steiner, H. Höchst, W. Steffen, and S. Hüfner, Z. Phys. B **38**, 191 (1980).

[35] C. P. Flynn, D. A. Rigney, and J. A. Gardner, Philos. Mag. **15**, 1255 (1967).